


Article

Description for $N = 126$ Isotones ^{210}Po and ^{212}Rn with Particle-Hole Excited Nucleon-Pair Approximation and Realistic Effective Interaction

Yi-Xing Wang ¹, Yi-Yuan Cheng ^{1,*}  and Thomas T. S. Kuo ²¹ Department of Physics, East China Normal University, Shanghai 200241, China; 51194700002@stu.ecnu.edu.cn² Department of Physics and Astronomy, Stony Brook University, New York, NY 11794-3800, USA; kuo@tonic.physics.sunysb.edu

* Correspondence: yycheng@phy.ecnu.edu.cn

Abstract: In this paper, we study yrast states of two $N = 126$ isotones ^{210}Po and ^{212}Rn using the nucleon-pair approximation with particle-hole excitations and using a low-momentum interaction $V_{\text{low-}k}$ renormalized from the free CD-Bonn NN potential. An overall good agreement with experimental level structures, $B(E2)$ s, and $B(E3)$ s, is achieved. We also calculate the probabilities of neutron particle-hole excitations in these yrast states, with a focus on negative-parity states, which reflect the roles played by the neutron negative-parity configurations of one-particle-one-hole excitations across the $N = 126$ shell gap and the negative-parity configurations of valence proton particles involving the $0i_{13/2}$ orbit. The $N = 126$ shell gap is discussed in terms of energies of neutron one-particle-one-hole excitations.

Keywords: $N = 126$ isotones; nucleon-pair approximation with particle-hole excitations; low-momentum interaction $V_{\text{low-}k}$



Citation: Wang, Y.-X.; Cheng, Y.-Y.; Kuo, T.T.S. Description for $N = 126$ Isotones ^{210}Po and ^{212}Rn with Particle-Hole Excited Nucleon-Pair Approximation and Realistic Effective Interaction. *Symmetry* **2022**, *14*, 181. <https://doi.org/10.3390/sym14010181>

Academic Editors: Yu-Gang Ma, De-Qing Fang and Fu-Rong Xu

Received: 30 September 2021

Accepted: 3 January 2022

Published: 17 January 2022

Publisher's Note: MDPI stays neutral with regard to jurisdictional claims in published maps and institutional affiliations.



Copyright: © 2022 by the authors. Licensee MDPI, Basel, Switzerland. This article is an open access article distributed under the terms and conditions of the Creative Commons Attribution (CC BY) license (<https://creativecommons.org/licenses/by/4.0/>).

1. Introduction

$N = 126$ isotones have been of great importance and interest in both experimental and theoretical studies. One of the key issues is the shell structure in these nuclei, i.e., the robustness of the $N = 126$ shell gap and the existence of the foreseen $Z = 92$ subshell. Important experimental progresses have been made along this line in recent years; see, e.g., [1–7]. Theoretically, characterized by large model spaces and reflections of various correlations, the nuclei in the ^{208}Pb region are challenging subjects. Despite the challenge, nuclear shell-model calculations using effective interactions have been successful in describing a large amount of low-lying states for nuclei in this region, in particular for $N = 126$ isotones; see, e.g., References [8–16].

The first realistic effective interaction for this region is the Kuo–Herling (KH) interaction [8], which was derived from the Hamada–Johnston NN potential [17] using the method developed by Kuo and Brown [18,19]. In Reference [9], with the KH interaction, a good agreement with experimental data was achieved by the shell-model calculation for low-lying states of nuclei with two to four identical particles coupled to the ^{208}Pb core. In Reference [10], modifications to the KH interaction were made to find the best fit to the experimental energy spectra of $A = 204–206$ and $210–212$ nuclei. In References [11,12], a realistic effective interaction for the ^{208}Pb region was derived from the Bonn-A NN potential [20] using the Brueckner G -matrix method followed by the \hat{Q} -box folded-diagram method [21,22], together with which the shell-model calculation provided a good description for the low-lying states of $^{206,205,204}\text{Pb}$ and $N = 126$ isotones ^{210}Po , ^{211}At , ^{212}Rn . In Reference [14], a large-scale shell-model calculation with the modified KH interaction [8,10] gave a good description to the low-lying states of the $N = 126$ isotones Po–Pu. Very recently, in Reference [16], a shell-model study with a realistic effective interaction derived from the CD-Bonn potential [23] using the $V_{\text{low-}k}$ method [24–26] followed by the \hat{Q} -box

method [21,22], provided a good description for the low-lying states of Pb, Po, Rn, Ra, and Th nuclei with $126 \leq N \leq 134$.

The neutron particle–hole excitations across the $N = 126$ shell gap are expected to play an important role in the low-lying states of $N = 126$ isotones, especially in the negative-parity states. In Reference [13], a shell-model study for the low-lying states of the doubly magic ^{208}Pb nucleus, where the model space consists of particle–hole excitations up to two-particle-two-hole excitations, well reproduced the available experimental data. Yet, for other $N = 126$ isotones with $Z \neq 82$, the shell-model spaces including configurations of such particle–hole excitations are too large.

In this work, we calculate the low-lying states of the $N = 126$ isotones ^{210}Po and ^{212}Rn using the nucleon-pair approximation with particle–hole excitations [27], together with the low-momentum interaction $V_{\text{low}-k}$ [24–26] derived from the free CD-Bonn potential [23]. The configurations of neutron particle–hole excitations across the $N = 126$ shell gap are included. We focus on the negative-parity states and study the roles played by the negative-parity configurations of valence protons involving the $0i_{13/2}$ orbit and the neutron negative-parity configurations of one-particle-one-hole excitations across the $N = 126$ shell gap.

The nucleon-pair approximation (NPA) [28,29] is a pair-truncation scheme of the shell model based on the technique of calculating the commutators between coupled fermion clusters [30,31]. Such a pair-truncation scheme with optimized pair structures is shown to be able to give a good description to low-lying states of semi-magic nuclei, transitional nuclei, and well-deformed nuclei; see, e.g., References [32–44]. For a comprehensive review, see Reference [45]. In recent years, the NPA with isospin symmetry [46], the version with particle–hole excitations [27], and the versions considering pairs in the M -scheme [47,48] have been developed. In the NPA with particle–hole excitations [27], a particle–hole “mixed” representation is adopted, where the particle–hole conjugate transformation is applied to the operators of the lower major shell while the operators of the upper major shell remain unchanged, so that three types of collective pairs, i.e., particle–particle, hole–hole, and particle–hole pairs, are equally treated in technique.

This paper is organized as follows. In Section 2, we briefly introduce the pair configuration space of particle–hole excitations and the shell-model Hamiltonian we use. In Section 3, we present and discuss our calculated results of energy levels, $B(E2)$ s, and $B(E3)$ s, in comparison with experimental data, as well as probabilities of neutron particle–hole excitations in the discussed states. We also discuss the $N = 126$ shell gap in terms of energies of neutron one-particle-one-hole excitations. In Section 4, we summarize the paper.

2. Theoretical Framework

2.1. Pair Configuration Space of Particle–Hole Excitations

The vacuum state in our particle–hole mixed representation corresponds to the state of the fully filled lower major shell in the particle representation. In the mixed representation, the operators that create collective particle–particle (pp), hole–hole (hh), and particle–hole (ph) pairs are all in the same form as below:

$$A^{(r)\dagger} \equiv A_{\mu}^{(r)\dagger} = \sum_{j_1 j_2} y(j_1 j_2 r) A^{(r)\dagger}(j_1 j_2),$$

$$A^{(r)\dagger}(j_1 j_2) \equiv A_{\mu}^{(r)\dagger}(j_1 j_2) = \left(a_{j_1}^{\dagger} \times a_{j_2}^{\dagger} \right)_{\mu}^{(r)}. \quad (1)$$

Here, $A^{(r)\dagger}(j_1 j_2)$ is a non-collective pair, and $\left(a_{j_1}^{\dagger} \times a_{j_2}^{\dagger} \right)_{\mu}^{(r)} = \sum_{m_1 m_2} C_{j_1 m_1 j_2 m_2}^{r\mu} a_{j_1 m_1}^{\dagger} a_{j_2 m_2}^{\dagger}$ with $C_{j_1 m_1 j_2 m_2}^{r\mu}$ the Clebsch–Gordan coefficient. We denote the creation operator of the orbit associated with quantum numbers (n, l, j, m) by using $a_{jm}^{\dagger} \equiv a_{nljm}^{\dagger}$. The collective pair $A^{(r)\dagger}$ is given by a linear combination of all non-collective pairs with spin r , and $y(j_1 j_2 r)$ is the so-called structure coefficient.

Let us use j_1, j_2, \dots, j_n to label orbits in the upper major shell and $j_{n+1}, j_{n+2}, \dots, j_{n+m}$ to label orbits in the lower major shell, and then the structure-coefficient matrices of the pp, hh, ph pairs are in the following form:

$$y_{pp} = \begin{pmatrix} A_{n \times n} & \mathbf{0} \\ \mathbf{0} & \mathbf{0} \end{pmatrix}, \quad y_{hh} = \begin{pmatrix} \mathbf{0} & \mathbf{0} \\ \mathbf{0} & B_{m \times m} \end{pmatrix}, \quad y_{ph} = \begin{pmatrix} \mathbf{0} & C_{n \times m} \\ \mathbf{0} & \mathbf{0} \end{pmatrix}, \quad (2)$$

where the subscripts “pp”, “hh”, and “ph” refer to pp, hh, and ph pairs, respectively. Note that the particle–hole pair acting on the vacuum state in the mixed representation corresponds to the phonon excitation with respect to the fully filled lower major shell in the particle representation.

Pair basis states are constructed by collective pair creation operators coupled successively and acting on the vacuum state. In this work, we consider neutron particle–hole excitations across the $N = 126$ shell gap up to two-particle-two-hole (2p2h) excitations, and construct such neutron configuration spaces using low-lying particle–hole pairs. Thus, neutron basis states in this work are in the forms as below:

$$0p0h : |0\rangle, \quad 1p1h : A_{ph}^{(r_1)\dagger} |0\rangle, \quad 2p2h : [A_{ph}^{(r_1)\dagger} \times A_{ph}^{(r_2)\dagger}]^{(J)} |0\rangle, \quad (3)$$

where the subscript “ph” refers to the ph pair.

2.2. Shell-Model Hamiltonian with the Effective Interaction

In the particle representation, the shell-model Hamiltonian with the effective interaction can be expressed to be the sum of the proton part, neutron part and proton–neutron part as below:

$$\begin{aligned} H &= \sum_{\sigma=\pi,\nu} H_{\sigma} + H_{\pi\nu}, \\ H_{\sigma} &= \sum_j \varepsilon_j (n_j)_{\sigma} + \sum_{j_1 \leq j_2} \sum_{j_3 \leq j_4} \sum_J \frac{V_{JT=1}(j_1 j_2 j_3 j_4)}{\sqrt{(1 + \delta_{j_1 j_2})(1 + \delta_{j_3 j_4})}} \hat{J} \left((A^{(J)\dagger}(j_1 j_2))_{\sigma} \times (\tilde{A}^{(J)}(j_3 j_4))_{\sigma} \right)^{(0)}, \\ H_{\pi\nu} &= - \sum_{j_1 j_2} \sum_{j_3 j_4} \sum_J V_J^{\pi\nu}(j_1 j_2 j_3 j_4) \hat{J} \left((a_{j_1}^{\dagger})_{\pi} \times (a_{j_2}^{\dagger})_{\nu} \right)^{(J)} \times \left((\tilde{a}_{j_3})_{\pi} \times (\tilde{a}_{j_4})_{\nu} \right)^{(J)} \right)^{(0)}, \\ V_J^{\pi\nu}(j_1 j_2 j_3 j_4) &= \frac{1}{2} (V_{JT=1}(j_1 j_2 j_3 j_4) + V_{JT=0}(j_1 j_2 j_3 j_4)) \sqrt{(1 + \delta_{j_1 j_2})(1 + \delta_{j_3 j_4})}. \end{aligned} \quad (4)$$

Here, $\hat{J} = \sqrt{2J+1}$; $n_j = \sum_m a_{jm}^{\dagger} a_{jm}$, and $A^{(J)\dagger}(j_1 j_2)$ is given in Equation (1); \tilde{a}_{jm} is the time-reversed operator of the single-particle destruction, and we use the convention $\tilde{a}_{jm} = (-)^{j-m} a_{j,-m}$. We use ε_j to denote the single-particle energy, use $V_{JT=1}(j_1 j_2 j_3 j_4)$ to denote the normalized two-body matrix element of the isovector interaction, and use $V_{JT=0}(j_1 j_2 j_3 j_4)$ to denote the normalized two-body matrix element of the isoscalar interaction.

In the NPA calculation we further express $H_{\pi\nu}$ in terms of proton–neutron multipole–multipole interactions as follows: Denoting $(j_1)_{\pi} \equiv j_{\pi}$, $(j_2)_{\nu} \equiv j_{\nu}$, $(j_3)_{\pi} \equiv j'_{\pi}$, $(j_4)_{\nu} \equiv j'_{\nu}$,

$$\begin{aligned} H_{\pi\nu} &= \sum_{j_{\pi} j'_{\pi}} \sum_{j_{\nu} j'_{\nu}} \sum_k \left(\sum_J (-)^{J+j_{\nu}+j'_{\pi}} (2J+1) \left\{ \begin{matrix} j_{\pi} & j_{\nu} & J \\ j'_{\nu} & j'_{\pi} & k \end{matrix} \right\} V_J^{\pi\nu}(j_{\pi} j_{\nu} j'_{\pi} j'_{\nu}) \right) \times \\ &\quad (-)^k \hat{k} \left(Q^{(k)}(j_{\pi} j'_{\pi}) \times Q^{(k)}(j_{\nu} j'_{\nu}) \right)^{(0)}, \end{aligned} \quad (5)$$

where $Q_{\kappa}^{(k)}(jj') = (a_j^{\dagger} \times \tilde{a}_{j'})_{\kappa}^{(k)}$. We first calculate the reduced matrix elements $\langle \| Q^k(j_{\pi} j'_{\pi}) \| \rangle$ and $\langle \| Q^k(j_{\nu} j'_{\nu}) \| \rangle$, and then calculate the matrix element of $\left(Q^{(k)}(j_{\pi} j'_{\pi}) \times Q^{(k)}(j_{\nu} j'_{\nu}) \right)^{(0)}$.

In the NPA with particle–hole excitations, we first transform the shell-model Hamiltonian in the particle representation (in the form as above) into the one in the particle–hole mixed representation. Then, we calculate the matrix elements of the Hamiltonian between pair basis states in the mixed representation.

3. Results and Discussions

In this work, we perform calculations for the yrast states of ^{210}Po and ^{212}Rn using the nucleon-pair approximation with particle–hole excitations [27], together with the low-momentum interaction $V_{\text{low-}k}$ [24–26]. We consider valence proton particles in the $(0h_{9/2}, 1f_{7/2}, 1f_{5/2}, 2p_{3/2}, 2p_{1/2}, 0i_{13/2})$ major shell, and neutron particle–hole excitations across the $N = 126$ shell gap with holes in the $(0h_{9/2}, 1f_{7/2}, 1f_{5/2}, 2p_{3/2}, 2p_{1/2}, 0i_{13/2})$ major shell and particles in the $(0i_{11/2}, 1g_{9/2}, 1g_{7/2}, 2d_{5/2}, 2d_{3/2}, 3s_{1/2}, 0j_{15/2})$ major shell.

Here, the low-momentum interaction $V_{\text{low-}k}$ [24–26] is renormalized from the CD-Bonn NN potential [23], with the decimation momentum $\Lambda = 2.3 \text{ fm}^{-1}$. For the two-body interaction matrix elements in the harmonic-oscillator single-particle basis, the parameter $\hbar\omega$ is set to be 6.88 MeV according to the formula $\hbar\omega = 45A^{-1/3} - 25A^{-2/3}$ [49] with $A = 208$. As we consider neutron particle–hole excitations across the $N = 126$ shell gap in this work, the shell-model effective Hamiltonian is for valence particles outside the $Z = 82, N = 82$ core. We use the two-body matrix elements of $V_{\text{low-}k}$ as our two-body effective interaction. Regarding single-particle energies with respect to the $Z = 82, N = 82$ core (denoted as ε_j), which, together with monopoles of $\langle |V_{\text{low-}k}| \rangle_s$, give corresponding single-particle energies with respect to the $Z = 82, N = 126$ core (denoted as e_j) as follows, we fix ε_j s to give e_j s that are consistent with those shown in Figure 1 of Reference [10].

$$\begin{aligned} e_{j_\pi} &= \varepsilon_{j_\pi} + \frac{1}{2j_\pi + 1} \sum_{j_{v0}} \sum_J (2J + 1) \langle j_\pi j_{v0} J | V_{\text{low-}k} | j_\pi j_{v0} J \rangle, \\ e_{j_\nu} &= \varepsilon_{j_\nu} + \frac{1}{2j_\nu + 1} \sum_{j_{v0}} \sum_J (2J + 1) (1 + \delta_{j_{v0}, j_\nu}) \langle j_{v0} j_\nu J | V_{\text{low-}k} | j_{v0} j_\nu J \rangle, \end{aligned} \quad (6)$$

where j_π represents an orbit in the proton $82 - 126$ major shell, j_{v0} represents an orbit in the lower neutron major shell below $N = 126$, and j_ν represents an orbit either in the lower neutron major shell or in the higher neutron major shell.

To eliminate in low-lying states the contributions of the spurious states arising from the center-of-mass motion, we use the Gloeckner–Lawson method [50], where a center-of-mass Hamiltonian was added to push up the expectation energies of the spurious states as follows:

$$H = H_{\text{SM}} + \beta \left(H_{\text{CM}} - \frac{3}{2} \hbar\omega \right), \quad H_{\text{CM}} = \frac{\tilde{P}^2}{2mA} + \frac{1}{2} mA\omega^2 \tilde{R}^2, \quad (7)$$

where H_{SM} is the shell-model Hamiltonian; A is the mass number of the calculated nucleus, and \tilde{P} and \tilde{R} are the center-of-mass momentum and coordinate, respectively. In our calculation, the parameter $\beta\hbar\omega/A$ is set to be 5 MeV.

For the configuration space of ^{210}Po , we adopt the full space of valence proton particles, and construct the neutron configuration space consisting of particle–hole excitations up to two-particle-two-hole (2p2h) excitations using the low-lying particle–hole pairs (i.e., the phonons with respect to the $N = 126$ closed shell in the particle representation) with negative parity and with spin 2, 3, 4, 5, 6, 7, 8, respectively. For ^{212}Rn , we construct the proton configuration space using the five low-lying positive-parity pairs with spin 0, 2, 4, 6, 8, respectively, as well as the ten low-lying negative-parity pairs with spin 2, 3, ..., 11, respectively. According to our calculation the contributions of neutron 2p2h configurations in the discussed low-lying states of ^{210}Po are negligible; thus, for ^{212}Rn , we consider the neutron configuration space consisting of the $N = 126$ closed-shell state and the one-particle-one-hole (1p1h) configurations constructed using the same particle–hole pairs as those adopted for ^{210}Po .

Now, we present and discuss our calculated results. In Figure 1, we present the calculated energy levels of ^{210}Po in the upper panel and those of ^{212}Rn in the lower panel, in comparison with experimental data [4,51]. One can see in Figure 1 that our calculated results agree with experimental data reasonably. We shall compare our theoretical energy levels with experimental ones in detail later. In Table 1, we present the calculated transition probabilities $B(E2)$ s and $B(E3)$ s, in comparison with experimental data [51]. Regarding effective charges, for $E2$ transitions, we adopt $e_\pi(E2) = 1.5e$ and $e_\nu(E2) = 0.5e$, and for $E3$ transitions we adopt $e_\pi(E3) = 2.0e$ and $e_\nu(E3) = 1.0e$. One sees in Table 1 that a very good agreement with available experimental transition probabilities is achieved by our calculation.

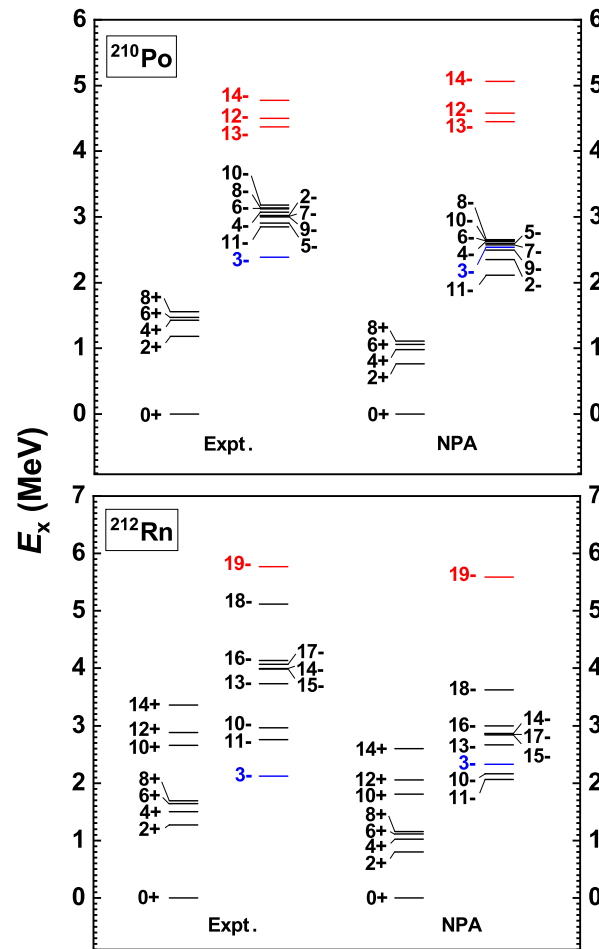


Figure 1. Calculated energy levels of ^{210}Po are in the upper panel and those of ^{212}Rn are in the lower panel, in comparison with experimental data [4,51]. In the calculation, we use the low-momentum interaction $V_{\text{low-}k}$ [24–26] renormalized from the CD-Bonn potential [23], as our two-body effective interaction. The adopted single-particle energies with respect to the $Z = 82$, $N = 82$ core, together with monopoles of $\langle |V_{\text{low-}k}| \rangle_s$, give corresponding single-particle energies with respect to the $Z = 82$, $N = 126$ core, as well as the $N = 126$ shell gap, consistent with Figure 1 of Reference [10]. We classify the discussed yrast states into three cases which are drawn in black, red, and blue, respectively. See the texts for details.

In Figure 2, we present the probability of neutron $1p1h$ excitations across the $N = 126$ shell gap in the yrast states, as well as the probability of the $N = 126$ closed-shell state. In our calculation, the contributions of neutron $2p2h$ configurations in the discussed low-lying states of ^{210}Po are all negligible. According to the results of Figure 2, we classify the yrast states into three cases as follows and present them in three colors in Figure 1.

- Case 1: the yrast states drawn in black, which are dominated by the configurations of valence proton particles coupled to the $N = 126$ closed shell.

- Case 2: the yrast states drawn in red, which are dominated by the configurations of valence proton particles with seniority $\nu \neq 0$ coupled to the neutron 1p1h configurations, i.e., to the neutron particle–hole pairs.
- Case 3: the 3_1^- state, which is drawn in blue.

Table 1. Calculated transition probabilities $B(EL; J_i^P \rightarrow J_f^P)$ s with $L = 2$ or 3 (in Weisskopf units), in comparison with experimental data [51]. We also present the shell-model results of References [12,14] for comparison; the results of Reference [12] by Coraggio and collaborators are denoted by “SM1” and the results of Reference [14] by Caurier and collaborators are denoted by “SM2”. In the calculations of SM1 and SM2, configurations of neutron particle–hole excitations were not considered. In our calculation, the initial and final states of the transitions listed here all belong to Case 1, i.e., are states dominated by valence proton configurations coupled to the $N = 126$ closed shell.

Nuclei	J_i^P	J_f^P	L	Expt.	This Work	SM1	SM2
^{210}Po	2_1^+	0_1^+	2	0.56 ± 0.12	3.60	3.55	3.55
	4_1^+	2_1^+	2	4.46 ± 0.18	4.37	4.46	4.51
	6_1^+	4_1^+	2	3.05 ± 0.09	3.00	3.07	3.09
	8_1^+	6_1^+	2	1.12 ± 0.04	1.21	1.25	1.24
	11_1^-	8_1^+	3	3.71 ± 0.10	1.64	0.55	0.89
^{212}Rn	2_1^+	0_1^+	2	-	5.81	-	6.41
	4_1^+	2_1^+	2	$1.050^{+0.044}_{-0.040}$	0.83	1.42	1.51
	6_1^+	4_1^+	2	$0.40^{+0.06}_{-0.04}$	0.47	0.73	0.83
	8_1^+	6_1^+	2	0.117 ± 0.007	0.17	0.252	0.26
	12_1^+	10_1^+	2	$4.52^{+0.32}_{-0.29}$	3.20	3.6	3.62
	17_1^-	15_1^-	2	$2.94^{+0.17}_{-0.15}$	2.71	2.9	2.87
	11_1^-	8_1^+	3	$1.8^{+0.6}_{-0.4}$	0.78	-	0.60
	17_1^-	14_1^+	3	$21.3^{+1.7}_{-1.5}$	20.90	6	20.41

Let us discuss Case 1 first. In the upper panel of Figure 1 for ^{210}Po , one sees that although the calculated energy levels of Case 1, i.e., those of $0_1^+, 2_1^+, \dots, 8_1^+$ and those of $2_1^-, 4_1^-, 5_1^-, \dots, 10_1^-, 11_1^-$, are lower than corresponding experimental ones, the relative level spacing given by the calculation is very similar to that given by the experimental data. The calculated $R_{I_1^+/2_1^+}$'s with $I = 4, 6, 8$, which are equal to (1.29, 1.39, 1.46), are very close to the experimental ones (1.21, 1.25, 1.32). For the negative-parity states, the calculated energy levels are close to each other, with the 11_1^- state being the lowest one, and so are the experimental ones.

Similarly, in the lower panel of Figure 1 for ^{212}Rn , one sees that although the calculated energy levels of Case 1 (in particular, the negative-parity ones), i.e., those of $0_1^+, 2_1^+, \dots, 14_1^+$ and those of $10_1^-, 11_1^-, 13_1^-, 14_1^-, \dots, 17_1^-, 18_1^-$, are lower than corresponding experimental data, the relative level spacing given by the calculation is very similar to that given by experimental data. The calculated $R_{I_1^-/11_1^-}$'s with $I = 10, 13, 14, \dots, 17, 18$, which are equal to (1.05, 1.29, 1.39, 1.38, 1.46, 1.38, 1.76), are very close to the experimental values (1.07, 1.35, 1.45, 1.45, 1.50, 1.47, 1.85).

In Table 1, the initial and final states of the discussed transitions all belong to Case 1, i.e., are dominated by the configurations of valence proton particles coupled to the $N = 126$ closed shell. One sees that the experimental transition probabilities are very well reproduced by our calculation, except for those of the $2_1^+ \rightarrow 0_1^+, 11_1^- \rightarrow 8_1^+$ transitions of ^{210}Po . In Table 1, we also present two sets of shell-model results [12,14] for comparison. In the two shell-model calculations [12,14], configurations of neutron particle–hole excitations were not considered. One sees that our results and the two sets of shell-model results are close to each other.

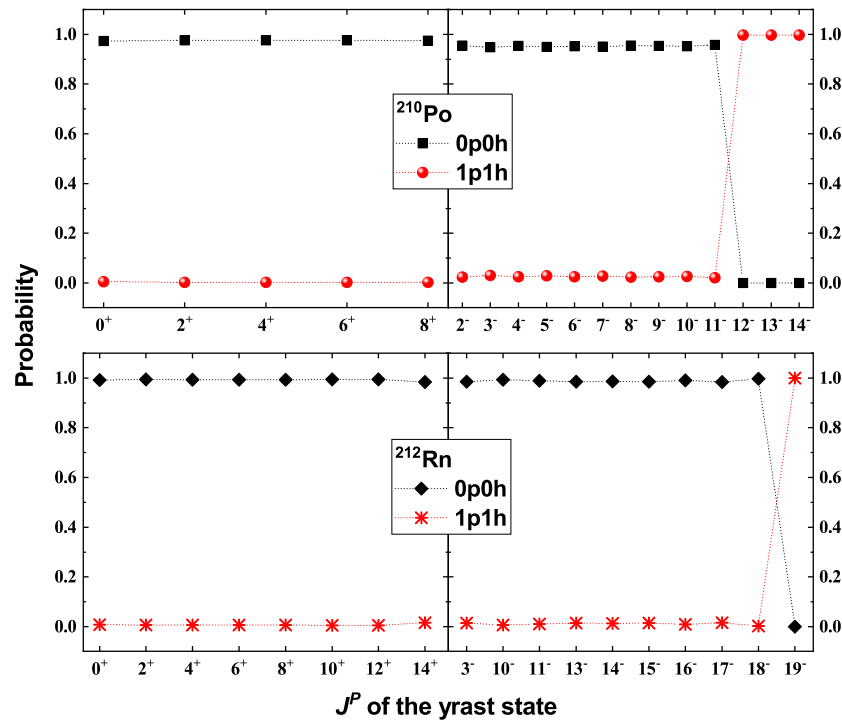


Figure 2. The probability of neutron one-particle-one-hole (1p1h) excitations across the $N = 126$ shell gap, as well as the probability of the closed-shell (i.e., 0p0h) state, in the yrast states of ^{210}Po and ^{212}Rn .

We then come to Case 2. These negative-parity states, i.e., 12_1^- , 13_1^- , 14_1^- of ^{210}Po and 19_1^- of ^{212}Rn , are dominated by the configurations of valence proton particles with seniority $\nu \neq 0$ coupled to the neutron 1p1h excitations across the $N = 126$ shell gap. In Figure 1, one sees that for both ^{210}Po and ^{212}Rn , the calculated energy levels of Case 2 are very close to the corresponding experimental ones. Yet, the comparison between the calculated energy levels of Case 1 and experimental ones in Figure 1 reflects that the calculated excitation energies of valence proton configurations of seniority $\nu \neq 0$ with respect to the proton $\nu = 0$ state might be lower than the ones inferred from experimental data, and then energies of neutron 1p1h excitations across the $N = 126$ shell gap in the calculation might be higher than the ones inferred from experimental data.

We then decrease the $N = 126$ shell gap and perform more NPA calculations with configuration spaces constructed in the same way as in the previous calculation. As shown in Figure 2, in our previous calculation the 12_1^- , 13_1^- , 14_1^- states of ^{210}Po and the 19_1^- state of ^{212}Rn almost purely consist of configurations of neutron 1p1h excitations. Thus, with a decrease in the $N = 126$ shell gap, the calculated wave functions of these states will approximately not change, while the calculated energies will approximately decrease by the same amount. Furthermore, according to our calculation, the 12_1^- , 13_1^- , 14_1^- states of ^{210}Po almost purely consist of neutron 1p1h excitations coupled to the proton configurations with $(J^P)_\pi = 8^+$, and the 19_1^- state of ^{212}Rn almost purely consists of neutron 1p1h excitations coupled to the proton configurations with $(J^P)_\pi = 14^+$. Thus, as an approximation, we regard the 12_1^- , 13_1^- , 14_1^- states of ^{210}Po to be neutron 1p1h excited states with respect to the 8_1^+ state, and the 19_1^- state of ^{212}Rn to be a neutron 1p1h excited state with respect to the 14_1^+ state. We further use $\Delta E_1 = E(12_1^-) - E(8_1^+)$ and $\Delta E_2 = E(13_1^-) - E(8_1^+)$ of ^{210}Po , as well as $\Delta E_3 = E(19_1^-) - E(14_1^+)$ of ^{212}Rn , to represent the energies of corresponding neutron 1p1h excitations, and present them versus the change of the $N = 126$ shell gap in Figure 3. One sees in Figure 3 that the calculated ΔE_1 , ΔE_2 , ΔE_3 with the decreasing shell gap indeed follow straight lines with the same slope. Furthermore, one sees that, after decreasing the $N = 126$ shell gap by 0.6 MeV, (i.e., with the shell gap in the ^{208}Pb core

being $\Delta'_{\text{sh}} = \Delta_{\text{sh}} - 0.6 = 2.83$ MeV), the calculated energies of neutron 1p1h excitations are consistent with the ones inferred from experimental data.

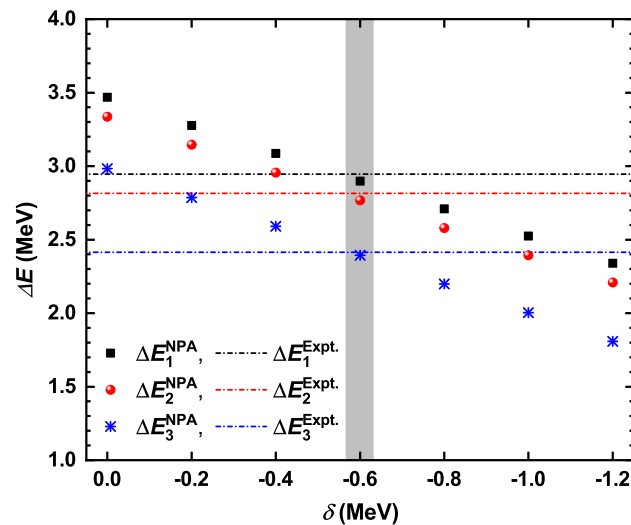


Figure 3. The energy differences (in units of MeV), $\Delta E_1 = E(12_1^-) - E(8_1^+)$ and $\Delta E_2 = E(13_1^-) - E(8_1^+)$ of ^{210}Po , as well as $\Delta E_3 = E(19_1^-) - E(14_1^+)$ of ^{212}Rn , which we use to represent the energies of corresponding neutron 1p1h excitations, versus the change of the $N = 126$ shell gap (denoted as δ and in units of MeV) adopted in the calculation. In all the calculations, the configuration spaces are constructed in the same way. For comparison, we also present the corresponding experimental values. See the texts for details.

Last, we discuss the 3_1^- state. Neutron particle–hole excitations are expected to play an essential role in these 3_1^- states. Yet, in our calculation where the $N = 126$ shell gap consistent with Figure 1 of Reference [10] is adopted, the 3_1^- states of ^{210}Po and ^{212}Rn are both dominated by the negative-parity configurations of valence proton particles coupled to the $N = 126$ closed shell. As discussed above, we also decrease the $N = 126$ shell gap and perform more NPA calculations. As shown in Figure 3, after decreasing the shell gap by 0.6 MeV, the calculated energy differences which we use to represent the energies of corresponding neutron 1p1h excitations, are very close to experimental data. However, according to our calculation, after decreasing the shell gap by 0.6 MeV, the 3_1^- states are still dominated by valence proton configurations coupled to the $N = 126$ closed shell. This might be a consequence of the argument discussed previously, i.e., that the excitation energies of valence proton configurations of seniority $\nu \neq 0$ with respect to the proton $\nu = 0$ state in our calculation are lower than those inferred from experimental data. In a future work, we intend to further investigate these 3_1^- states with a new effective interaction for the proton part, to be derived by using the $V_{\text{low-}k}$ method [24–26] followed by the \hat{Q} -box method [21,22].

4. Summary

In this paper, we study the yrast states of two $N = 126$ isotones, ^{210}Po and ^{212}Rn , using the nucleon-pair approximation with particle–hole excitations, and using a low-momentum interaction $V_{\text{low-}k}$ renormalized from the realistic CD-Bonn potential. We consider valence proton particles in the 82–126 major shell and neutron particle–hole excitations across the $N = 126$ shell gap with holes in the 82–126 major shell and particles in the 126–184 major shell. The configurations of neutron particle–hole excitations are constructed using the low-lying particle–hole pairs. Note that the particle–hole pairs in our particle–hole mixed representation correspond to the phonon excitations with respect to the fully filled lower major shell in the particle representation. An overall good agreement with experimental level structures, $B(E2)$ s, and $B(E3)$ s, is achieved.

According to our calculation where the adopted single-particle energies are consistent with Figure 1 of Reference [10], most yrast states discussed here are dominated by the

configurations of valence proton particles coupled to the $N = 126$ closed shell, while the 12_1^- , 13_1^- , 14_1^- states of ^{210}Po and the 19_1^- state of ^{212}Rn are dominated by the configurations of valence proton particles with seniority $\nu \neq 0$ coupled to the neutron one-particle-one-hole (1p1h) excitations across the $N = 126$ shell gap. The comparison between our calculated energy levels and experimental ones indicates that the excitation energies of valence proton configurations of seniority $\nu \neq 0$ with respect to the proton $\nu = 0$ state in our calculation might be lower than those inferred from experimental data; meanwhile, the excitation energies of neutron 1p1h excitations across the $N = 126$ shell gap in the calculation might be higher than those inferred from experimental data.

We then decrease the $N = 126$ shell gap and perform more NPA calculations with configuration spaces constructed in the same way as in the above calculation. Our results suggest that, after decreasing the shell gap by 0.6 MeV, the calculated energy differences, which we use to represent the energies of corresponding neutron 1p1h excitations, are very close to the experimental data, while the 3_1^- states are still dominated by valence proton configurations coupled to the $N = 126$ closed shell. In a future work, we intend to further investigate these 3_1^- states with a new effective interaction for the proton part, to be derived by using the $V_{\text{low}-k}$ method followed by the \hat{Q} -box method.

Author Contributions: Methodology, Y.-Y.C. and T.T.S.K.; investigation, Y.-Y.C. and Y.-X.W.; data curation, Y.-X.W. All authors have read and agreed to the published version of the manuscript.

Funding: This research was funded by the National Natural Science Foundation of China under Grant No. 11875134 and by the U.S. Department of Energy under Grant No. DE-FG02-88ER40388.

Institutional Review Board Statement: Not applicable.

Informed Consent Statement: Not applicable.

Data Availability Statement: Data is contained within the article.

Acknowledgments: The authors are grateful to Yu-Min Zhao for fruitful discussions.

Conflicts of Interest: The authors declare no conflict of interest.

References

- Hauschild, K.; Rejmund, M.; Grawe, H.; Caurier, E.; Nowacki, F.; Becker, F.; Le Coz, Y.; Korten, W.; Döring, J.; Górska, M.; et al. Isomer Spectroscopy in $^{216}\text{Th}_{126}$ and the Magicity of $^{218}\text{U}_{126}$. *Phys. Rev. Lett.* **2001**, *87*, 072501. [\[CrossRef\]](#)
- Andreyev, A.N.; Huyse, M.; Van Duppen, P.; Qi, C.; Liotta, R.J.; Antalic, S.; Ackermann, D.; Franchoo, S.; Heßberger, F.P.; Hofmann, S.; et al. Signatures of the $Z = 82$ Shell Closure in α -Decay Process. *Phys. Rev. Lett.* **2013**, *110*, 242502. [\[CrossRef\]](#)
- Khuyagbaatar, J.; Yakushev, A.; Düllmann, C.E.; Ackermann, D.; Andersson, L.-L.; Block, M.; Brand, H.; Cox, D.M.; Even, J.; Forsberg, U.; et al. New Short-Lived Isotope ^{221}U and the Mass Surface Near $N = 126$. *Phys. Rev. Lett.* **2015**, *115*, 242502. [\[CrossRef\]](#)
- Li, C.B.; Zhang, G.L.; Yuan, C.X.; Zhang, G.X.; Hu, S.P.; Qu, W.W.; Zheng, Y.; Zhang, H.Q.; Mengoni, D.; Testov, D.; et al. New level scheme and shell model description of ^{212}Rn . *Phys. Rev. C* **2020**, *101*, 044313. [\[CrossRef\]](#)
- Ma, L.; Zhang, Z.Y.; Gan, Z.G.; Zhou, X.H.; Yang, H.B.; Huang, M.H.; Yang, C.L.; Zhang, M.M.; Tian, Y.L.; Wang, Y.S.; et al. Short-Lived α -Emitting Isotope ^{222}Np and the Stability of the $N = 126$ Magic Shell. *Phys. Rev. Lett.* **2020**, *125*, 032502. [\[CrossRef\]](#)
- Zhang, Z.Y.; Gan, Z.G.; Yang, H.B.; Ma, L.; Huang, M.H.; Yang, C.L.; Zhang, M.M.; Tian, Y.L.; Wang, Y.S.; Sun, M.D.; et al. New Isotope ^{220}Np : Probing the Robustness of the $N = 126$ Shell Closure in Neptunium. *Phys. Rev. Lett.* **2019**, *122*, 192503. [\[CrossRef\]](#)
- Zhang, Z.Y.; Yang, H.B.; Huang, M.H.; Gan, Z.G.; Yuan, C.X.; Qi, C.; Andreyev, A.N.; Liu, M.L.; Ma, L.; Zhang, M.M.; et al. New α -Emitting Isotope ^{214}U and Abnormal Enhancement of α -Particle Clustering in Lightest Uranium Isotopes. *Phys. Rev. Lett.* **2021**, *126*, 152502. [\[CrossRef\]](#)
- Herling, G.H.; Kuo, T.T.S. Two-particle states in ^{210}Pb , ^{210}Bi and ^{210}Po with realistic forces. *Nucl. Phys. A* **1972**, *181*, 113–131. [\[CrossRef\]](#)
- Mc Grory, J.B.; Kuo, T.T.S. Shell model calculations of two to four identical-“particle” systems near ^{208}Pb . *Nucl. Phys. A* **1975**, *247*, 283–316. [\[CrossRef\]](#)
- Warburton, E.K.; Brown, B.A. Appraisal of the Kuo-Herling shell-model interaction and application to $A = 210$ – 212 nuclei. *Phys. Rev. C* **1991**, *43*, 602. [\[CrossRef\]](#)
- Coraggio, L.; Covello, A.; Gargano, A.; Itaco, N.; Kuo, T.T.S. Bonn potential and shell-model calculations for $^{206,205,204}\text{Pb}$. *Phys. Rev. C* **1998**, *58*, 3346. [\[CrossRef\]](#)

12. Coraggio, L.; Covello, A.; Gargano, A.; Itaco, N.; Kuo, T.T.S. Bonn potential and shell-model calculations for $N = 126$ isotones. *Phys. Rev. C* **1999**, *60*, 064306. [[CrossRef](#)]
13. Brown, B.A. Double-Octupole States in ^{208}Pb . *Phys. Rev. Lett* **2000**, *85*, 5300. [[CrossRef](#)]
14. Caurier, E.; Rejmund, M.; Grawe, H. Large-scale shell model calculations for the $N = 126$ isotones Po-Pu. *Phys. Rev. C* **2003**, *67*, 054310. [[CrossRef](#)]
15. Qi, C.; Jia, L.Y.; Fu, G.J. Large-scale shell-model calculations on the spectroscopy of $N < 126$ Pb isotopes. *Phys. Rev. C* **2016**, *94*, 014312.
16. Naidja, H. New shell-model investigation of the lead-208 mass region: Spectroscopic properties and collectivity. *Phys. Rev. C* **2021**, *103*, 054303. [[CrossRef](#)]
17. Hamada, T.; Johnston, I.D. A potential model representation of two-nucleon data below 315 MeV. *Nucl. Phys.* **1962**, *34*, 382–403. [[CrossRef](#)]
18. Kuo, T.T.S.; Brown, G.E. Structure of finite nuclei and the free nucleon-nucleon interaction: An application to ^{18}O and ^{18}F . *Nucl. Phys.* **1966**, *85*, 40–86. [[CrossRef](#)]
19. Kuo, T.T.S.; Brown, G.E. Reaction matrix elements for the $0f-1p$ shell nuclei. *Nucl. Phys. A* **1968**, *114*, 241–279. [[CrossRef](#)]
20. Machleidt, R.; Holinde, K.; Elster, C. The bonn meson-exchange model for the nucleon-nucleon interaction. *Phys. Rep.* **1987**, *149*, 1–89. [[CrossRef](#)]
21. Kuo, T.T.S.; Lee, S.Y.; Ratcliff, K.F. A folded-diagram expansion of the model-space effective hamiltonian. *Nucl. Phys. A* **1971**, *176*, 65–88. [[CrossRef](#)]
22. Kuo, T.T.S.; Osnes, E. Folded-Diagram Theory of the Effective Interaction in Nuclei, Atoms and Molecules. *Lect. Notes Phys.* **1990**, *364*, 1–170.
23. Machleidt, R. High-precision, charge-dependent Bonn nucleon-nucleon potential. *Phys. Rev. C* **2001**, *63*, 024001. [[CrossRef](#)]
24. Bogner, S.K.; Kuo, T.T.S.; Coraggio, L.; Covello, A.; Itaco, N. Low momentum nucleon-nucleon potential and shell model effective interactions. *Phys. Rev. C* **2002**, *65*, 051301. [[CrossRef](#)]
25. Bogner, S.K.; Kuo, T.T.S.; Schwenk, A. Model-independent low momentum nucleon interaction from phase shift equivalence. *Phys. Rep.* **2003**, *386*, 1–27. [[CrossRef](#)]
26. Kuo, T.T.S.; Holt, J.W.; Osnes, E. Introduction to low-momentum effective interactions with Brown-Rho scaling and three-nucleon forces. *Phys. Scr.* **2016**, *91*, 033009. [[CrossRef](#)]
27. Cheng, Y.Y.; Zhao, Y.M.; Arima, A. Nucleon-pair approximation with particle-hole excitations. *Phys. Rev. C* **2018**, *97*, 024303.
28. Chen, J.Q. Nucleon-pair shell model: Formalism and special cases. *Nucl. Phys. A* **1997**, *626*, 686–714. [[CrossRef](#)]
29. Zhao, Y.M.; Yoshinaga, N.; Yamaji, S.; Chen, J.Q.; Arima, A. Nucleon-pair approximation of the shell model: Unified formalism for both odd and even systems. *Phys. Rev. C* **2000**, *62*, 014304. [[CrossRef](#)]
30. Chen, J.Q.; Chen, B.Q.; Klein, A. Factorization of commutators: The Wick theorem for coupled operators. *Nucl. Phys. A* **1993**, *554*, 61–76.
31. Chen, J.Q. The Wick theorem for coupled fermion clusters. *Nucl. Phys. A* **1993**, *562*, 218–240. [[CrossRef](#)]
32. Luo, Y.A.; Chen, J.Q. Shell model calculation in the S-D subspace. *Phys. Rev. C* **1998**, *58*, 589.
33. Zhao, Y.M.; Yamaji, S.; Yoshinaga, N.; Arima, A. Nucleon pair approximation of the nuclear collective motion. *Phys. Rev. C* **2000**, *62*, 014315. [[CrossRef](#)]
34. Zhao, Y.M.; Yoshinaga, N.; Yamaji, S.; Arima, A. Validity of the SD-pair truncation of the shell model. *Phys. Rev. C* **2000**, *62*, 014316. [[CrossRef](#)]
35. Jia, L.Y.; Zhang, H.; Zhao, Y.M. Systematic calculations of low-lying states of even-even nuclei within the nucleon pair approximation. *Phys. Rev. C* **2007**, *75*, 034307. [[CrossRef](#)]
36. Lei, Y.; Xu, Z.Y.; Zhao, Y.M.; Arima, A. Validity of pair truncations with effective interaction in Ca isotopes. *Phys. Rev. C* **2010**, *82*, 034303. [[CrossRef](#)]
37. Lei, Y.; Zhao, Y.M.; Arima, A. Validity of pair approximations for nuclei in open shells. *Phys. Rev. C* **2011**, *84*, 044301. [[CrossRef](#)]
38. Jiang, H.; Lei, Y.; Fu, G.J.; Zhao, Y.M.; Arima, A. $B(E2; 0_1^+ \rightarrow 2_1^+)$ values of even-even Sn isotopes. *Phys. Rev. C* **2012**, *86*, 054304. [[CrossRef](#)]
39. Jiang, H.; Lei, Y.; Qi, C.; Liotta, R.; Wyss, R.; Zhao, Y.M. Magnetic moments of low-lying states in tin isotopes within the nucleon-pair approximation. *Phys. Rev. C* **2014**, *89*, 014320. [[CrossRef](#)]
40. Cheng, Y.Y.; Zhao, Y.M.; Arima, A. Nucleon-pair states of even-even $N = 82$ isotones. *Phys. Rev. C* **2016**, *94*, 024307. [[CrossRef](#)]
41. Cheng, Y.Y.; Wang, H.; Shen, J.J.; Zhou, X.R.; Zhao, Y.M.; Arima, A. Nucleon-pair picture of low-lying states in semi-magic and open-shell nuclei. *Phys. Rev. C* **2019**, *100*, 024321. [[CrossRef](#)]
42. Bao, Y.; Cheng, Y.Y.; Zhou, X.R. Quadrupole phonon excitations and transition probabilities for low-lying states of neutron-rich Cd isotopes. *Phys. Rev. C* **2021**, *104*, 034312. [[CrossRef](#)]
43. Fu, G.J.; Johnson, C.W. From deformed Hartree-Fock to the nucleon-pair approximation. *Phys. Lett. B* **2020**, *809*, 135705. [[CrossRef](#)]
44. Fu, G.J.; Johnson, C.W.; Van Isacker, P.; Ren, Z.Z. Nucleon-pair coupling scheme in Elliott's SU(3) model. *Phys. Rev. C* **2021**, *103*, L021302. [[CrossRef](#)]
45. Zhao, Y.M.; Arima, A. Nucleon-pair approximation to the nuclear shell model. *Phys. Rep.* **2014**, *545*, 1. [[CrossRef](#)]
46. Fu, G.J.; Lei, Y.; Zhao, Y.M.; Pittel, S.; Arima, A. Nucleon-pair approximation of the shell model with isospin symmetry. *Phys. Rev. C* **2013**, *87*, 044310. [[CrossRef](#)]

47. He, B.C.; Li, L.; Luo, Y.A.; Zhang, Y.; Pan, F.; Draayer, J.P. Nucleons pair shell model in M scheme. *Phys. Rev. C* **2020**, *102*, 024304. [[CrossRef](#)]
48. Lei, Y.; Lu, Y.; Zhao, Y.M. Nucleon-pair approximation with uncoupled representation. *Chin. Phys. C* **2021**, *45*, 054103. [[CrossRef](#)]
49. Blomqvist, J.; Molinari, A. Collective 0^- vibrations in even spherical nuclei with tensor forces. *Nucl. Phys. A* **1968**, *106*, 545–569. [[CrossRef](#)]
50. Gloeckner, D.H.; Lawson, R.D. Spurious center-of-mass motion. *Phys. Lett. B* **1974**, *53*, 313–318. [[CrossRef](#)]
51. Available online: <http://www.nndc.bnl.gov/ensdf/> (accessed on 28 September 2021).